A&A 457, 809–821 (2006)
DOI: 10.1051/0004-6361:20064845

Astronomy & Astrophysics

Stellar populations of early-type galaxies in different environments⋆

II. Ages and metallicities

P. Sánchez-Blázquez[1,2], J. Gorgas[2], N. Cardiel[2,3], and J. J. González[4]

[1] Laboratoire d'Astrophysique, École Polytechnique Fédérale de Lausanne (EPFL), Observatoire, 1290 Sauverny, Switzerland
e-mail: Patricia.SanchezBlazquez@epfl.ch
[2] Dpto. de Astrofísica, Fac. de Ciencias Físicas, Universidad Complutense de Madrid, 28040 Madrid, Spain
[3] Calar Alto Observatory, CAHA, Apartado 511, 04004 Almería, Spain
[4] Instituto de Astronomía, Universidad Nacional Autónoma de México, Apdo-Postal 70–264, México D.F, México

Received 11 January 2006 / Accepted 26 April 2006

ABSTRACT

Aims. This is the second paper of a series devoted to the study of the stellar content of early-type galaxies. The goal of the series is to set constraints on the evolutionary status of these objects
Methods. We use a new set of models that include an improved stellar library (MILES) to derive simple stellar population (SSP)-equivalent parameters in a sample of 98 early-type galaxies. The sample contains galaxies in the field, poor groups, and galaxies in the Virgo and Coma clusters.
Results. We find that low-density environment galaxies span a larger range in SSP age and metallicity than their counterparts in high density environments, with a tendency for lower σ galaxies to be younger. Early-type galaxies in low-density environments appear on average ∼1.5 Gyr younger and more metal rich than their counterparts in high density environments. The sample of low-density environment galaxies shows an age-metallicity relation in which younger galaxies are found to be more metal rich, but only when metallicity is measured with a Fe-sensitive index. Conversely, there is no age-metallicity relation when the metallicity is measured with a Mg sensitive index. The mass-metallicity relation is only appreciable for the low-density environment galaxies when the metallicity is measured with a Mg-sensitive index, and not when the metallicity is measured with other indicators. On the contrary, this relation exists for the high-density environment galaxies independent of the indicator used to measure the metallicity.
Conclusions. This suggests a dependence of the mass-metallicity relation on the environment of the galaxies. Our data favour a scenario in which galaxies in low density environments have suffered a more extended star formation history than the galaxies in the Coma cluster, which appear to host more homogenous stellar populations.

Key words. galaxies: abundances – galaxies: elliptical and lenticular, cD – Galaxy: stellar content – Galaxy: formation

1. Introduction

The knowledge of the star formation history of early-type galaxies is a key test of our understanding of the galaxy formation processes. The classic vision of elliptical galaxies as old objects forming their stars at high redshift in a single episode has been questioned by several studies of stellar population in these systems, which found a high fraction of early-type galaxies with apparent young ages (e.g., González 1993; Trager et al. 1998; Trager et al. 2000b; Terlevich & Forbes 2002; Sánchez-Blázquez 2004).

The semi-analytical models of galaxy formation (Kauffmann 1996; Baugh et al. 1996; Cole et al. 1994; Somerville et al. 1999; de Lucia et al. 2006), in the framework of the cold dark matter (CDM) cosmological model and in the current standard ΛCDM, predict extended star formation histories for early-type galaxies, with substantial fractions of the stellar population formed at relative low redshift, in agreement with the observed trends. The numerical simulations based on the semi-analytical models can impressively reproduce various features of large-scale structures from dwarf galaxies to giant galaxies and rich clusters of galaxies (e.g., Steinmetz & Navarro 2002; Klypin et al. 2003). One of the keys to test the hierarchical scenarios is to study the properties of galaxies situated in different environments, since the semi-analytical models predict that galaxies in dense clusters were assembled at higher redshift than galaxies in the field and poor groups. This is the second paper of a series devoted to the study of the stellar content in nearby early-type galaxies. The final aim of the series is to constrain the formation epoch of the stellar population in this kind of galaxies as a function of mass and environment. The first paper of the series (Sánchez-Blázquez et al. 2006a, hereafter Paper I) analysed the relation of the central line-strength indices with the velocity dispersion for a sample of 98 galaxies drawn from different environments. It also presented some evidence of differences in the stellar content of galaxies in different environments. In particular, we found that the index-σ relations are driven by both age and metallicity in the sample of galaxies in low-density environments and in the Virgo cluster. However, an age variation with σ is not required to explain the index-σ relations for galaxies belonging to the Coma cluster. We also presented evidence supporting the idea that the [Mg/Fe], [N/Fe], and probably [C/Fe] ratios increase with the velocity dispersion of the galaxy in both subsamples. In Paper I, we studied the scatter in

⋆ Table 1 is only available in electronic form at
http://www.edpsciences.org

the index-σ relations, finding that it is not only a consequence of a dispersion in the age of the galaxies, but that it is also due to variations of the [Mg/Fe] ratio. These variations are related to the mean ages of the galaxies, in the sense that younger galaxies exhibit, on average, lower [Mg/Fe] ratios. Furthermore, galaxies in the Coma cluster show, on average, higher [Mg/Fe] ratios than galaxies in lower environment. We also detected systematic differences in the values of some indices, which were interpreted as differences in chemical abundance ratios between both subsamples.

In Paper I we analysed the raw line-strength indices and their relation with other parameters. In this paper, we compare these indices with the predictions of the stellar population synthesis models by Vazdekis et al. (2006, in preparation, hereafter V06) to derive central simple stellar population (SSP) parameters for our sample of galaxies.

The outline of this paper is as follows. Section 2 details the estimation of age and metallicities. In Sect. 3 we study the mean values of these parameters and their differences as a function of the environment. In Sect. 4 we analyse the most likely scenarios to explain the dispersion in the ages of the galaxies. Section 5 presents a discussion of the age-metallicity relation for the galaxies in both environments, and in Sect. 6 we study the relation of the age and metallicity with the velocity dispersion. In Sect. 7 we present a brief discussion of the results, and Sect. 8 summarises our findings and conclusions.

The sample consists of 98 galaxies, out of which 35 belong to the rich cluster of Coma (high-density environment galaxies, hereafter HDEGs), and the rest are galaxies in the field, in groups or in the Virgo cluster (low-density environment galaxies, hereafter LDEGs). For a detailed description of the sample we refer the reader to Paper I.

2. Derivation of ages and metallicities

Previous works have used Lick/IDS line-strength indices to derive mean ages and metallicities using evolutionary synthesis models (e.g., Worthey 1994; Buzzoni 1995; Bruzual & Charlot 2003; Thomas et al. 2003). Here we follow a similar approach, deriving the SSP parameters (age and metallicity) by comparing the observed line-strengths with the predicted index-index diagrams from a new set of models by V06. These models are an updated version of those described by Vazdekis et al. (2003), improved by the inclusion of a new stellar library (MILES) recently observed by Sánchez-Blázquez et al. (2006b). This library contains 1003 stars, carefully selected to cover the atmospheric parameter space in an homogenous way. In particular, the library span a range of metallicities from [Fe/H] ~ -2.7 to +1.0 and a wide range of effective temperatures. The inclusion of this library reduces the uncertainties in the models, especially at metallicities departing from solar. Since the stars of the library are relatively flux calibrated, these models are able to predict not only individual features for a population of a given age and metallicity, but also the whole spectral energy distribution (SED). This allows us to analyse the spectra of the galaxies at their own resolution, given by their internal velocity and instrumental broadening (see, e.g., Vazdekis et al. 2001). The synthetic spectra have a spectral resolution of 2.4 Å and cover the spectral range 3500−7500 Å.

In spite of this capability, as we are using calibrations based on the Lick system, and to compare our results with previous studies, most of the analysis has been performed with the indices transformed into the Lick system. Therefore, we also broadened the synthetic spectra to match the wavelength dependent resolution of the Lick stellar library (Worthey & Ottaviani 1997) and measured the indices in the same way as in the galactic spectra. We then added the same offsets that we applied to the galaxy indices to the synthetic indices. (see Paper I for details).

Figure 1 shows several index-index diagrams combining different pairs of indices. Over-plotted are the stellar population models of V06 for various ages and metallicities, as indicated in the figure caption. Open and filled symbols represent LDEGs and HDEGs, respectively. It is clear from the figure that galaxies span a fair range in their mean ages. This result has been previously found by other authors (González 1993; Trager et al. 1998; Trager et al. 2000a), and it is in contradiction to the classical vision of early-type galaxies as old and coeval systems.

To quantify the age and metallicity values, we interpolated in the grids using bivariate polynomials, as described in Cardiel et al. (2003). Although the highest metallicity modeled by V06 is [M/H] = +0.2, to obtain metallicity values for the maximum number of galaxies, we extrapolated the predictions up to [M/H] = +0.5. However, all the values above [M/H] = +0.2 have to be considered more uncertain. The errors in age and metallicity were calculated as the differences between the central values and the values at the end of the error bars, which give an upper limit to the real errors. Table 5 lists the ages and metallicities derived from several index-index diagrams, all of them combining Hβ with other metal-sensitive indices. The empty spaces in the table indicate that the galaxy lies outside the model grid, and therefore no measurements of age and metallicity have been made. The ages and metallicities presented here represent simple stellar population equivalent parameters, and thus, if all the stars were not formed in a single event, they represent values weighted with the luminosity of the stars and do not necessarily reflect the age and the metallicity of the bulk of the stars in the galaxy. We have used Hβ as the main age indicator since the other higher-order Balmer lines (Hδ and Hγ) are very sensitive to α/Fe ratio changes at super-solar metallicities (Thomas et al. 2004).

2.1. The problem of the relative abundances

One aspect that is evident in Fig. 1 is that the ages and metallicities obtained with different indicators are not the same. In particular, the metallicities measured with indices such as CN_2, Mgb, and C4668 are larger than the metallicities measured with Fe-sensitive indices such as Fe4383. This effect has been noted previously by several authors (e.g., Peletier 1989; Faber et al. 1999; Vazdekis et al. 2001; Thomas et al. 2004, among others) and is commonly attributed to an overabundance of Mg (O'Connell 1976), N (Worthey 1998), and C (Vazdekis et al. 2001), with respect to Fe[1] compared to the solar abundance partition. The differences in the relative chemical abundance ratios with respect to the solar values is one of the major roadblocks to deriving reliable stellar population parameters. However, since different elements are produced in stars with different lifetimes, the study of the chemical composition of early-type galaxies is a powerful tool to disentangle the star formation history of these systems. Unfortunately, the computation of chemical abundances through comparisons with stellar population models is still in its infancy. Great efforts have been made to include

[1] Although we use the term overabundance, in fact Trager et al. (2000b) have shown that the differences are more likely due to a depression of Fe with respect to the solar values than to an enhancement of the light elements.

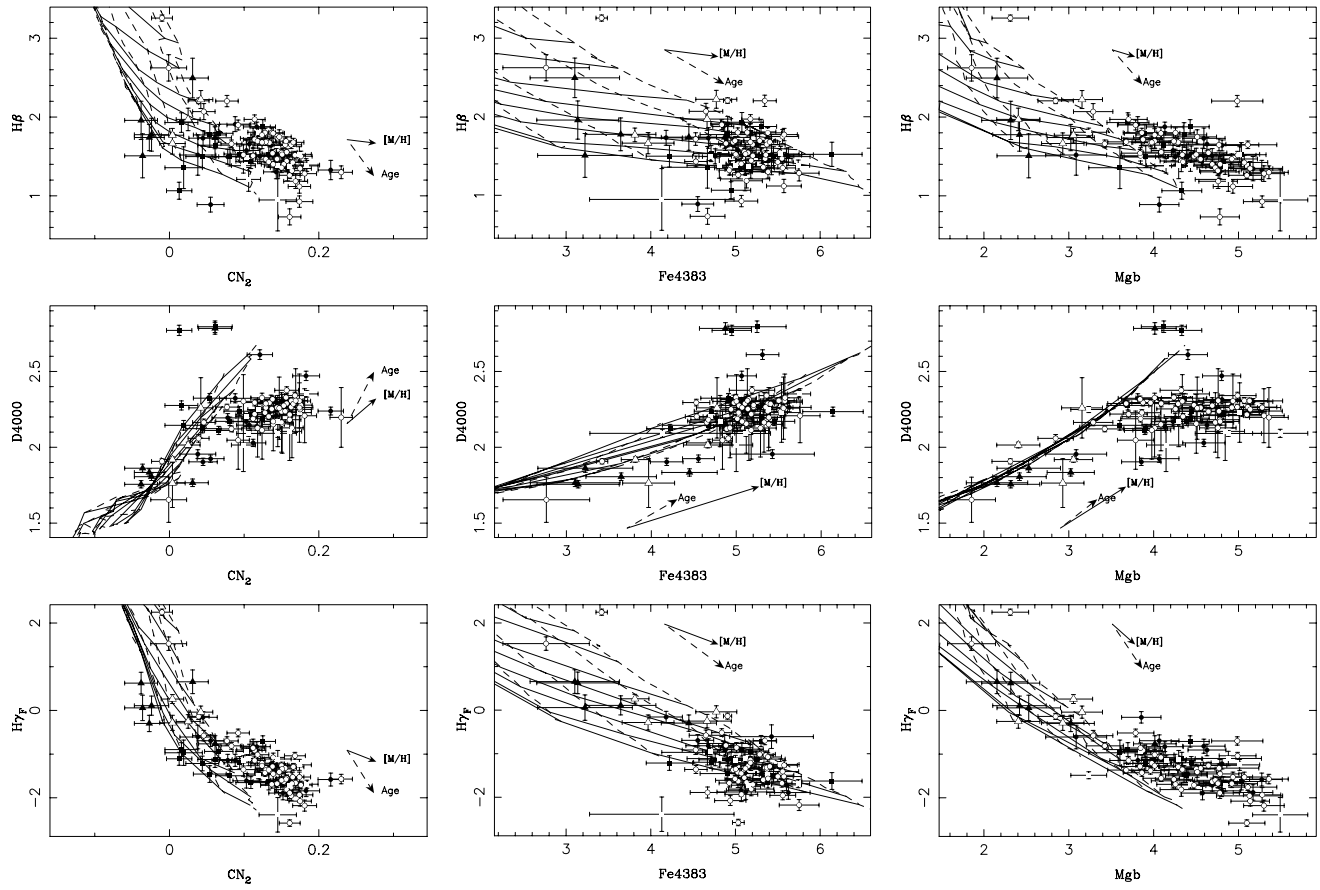

Fig. 1. Line strengths of LDEGs (open symbols) and HDEGs (filled symbols) through the central aperture. The distinct symbols indicate different kind of galaxies: triangles correspond to dwarf ellipticals, squares to lenticulars, and circles to normal ellipticals. Model grids from V06 have been superposed: solid lines are contours of constant age (1.0, 1.41, 2.00, 2.82, 3.98, 5.62, 7.98, 11.22, and 15.85 Gyr), and dashed lines are contours of constant [M/H] ([M/H] = −0.68, −0.38, 0.0, and +0.2 dex). The arrows indicate the direction of increasing age and metallicity. Three different metal indicators (CN_2, Fe4383, and Mgb) are combined with three different age-sensitive indexes (Hβ, D4000, and Hγ_F).

the non-solar partition effects in the theoretical models through the building of α-enhanced[2] isochrones (Salaris et al. 1993; Salasnich et al. 2000) and stellar model atmospheres with variations on the abundance of individual elements (Tripicco & Bell 1995). Some attempts have also been made to include these theoretical works into the SSP models (Trager et al. 2000b; Thomas et al. 2003). However, despite all this valuable work, we are still lacking models that include the effect of variations of chemical abundance ratios in a consistent way (with isochrones, model atmospheres, and stellar libraries). The current models have an inconsistency between the atmospheres and the stellar interiors.

The potential effects of including isochrones with non-solar chemical abundance ratios are not clear. Tantalo et al. (1998) built a set of stellar isochrones with relative abundances of [α/Fe] different than solar, and concluded that the models incorporating them were indistinguishable in the colour-magnitude diagram from the models with the same metallicity and [α/Fe] = 0. Salaris et al. (1993) showed (only for metallicities lower than solar) that the isochrones with overabundances of α elements were identical to the ones scaled to solar ratios at the same metallicity, if the ratio between the mass fraction of elements with high- and low- ionisation potential were constant. However, more recently, Salaris & Weiss (1998) have suggested that at higher metallicities (near solar), the isochrones shift to higher temperatures and their shapes change as the ratio α/Fe increases. Trager et al. (2000b) have analysed the effect of this change and have not found much difference in the predicted indices. However, Thomas & Maraston (2003) found large differences in the inferred ages using models that incorporate the isochrones with α-enhancement and the models that do not. So far, the effect of including isochrones with [C/Fe] and [N/Fe] different from solar has not been studied.

Another problem is that the empirical stellar libraries included in the population models are limited to stars in the solar neighbourhood with, therefore, relative compositions between different elements resembling the solar one. The ratios between the different elements in these stars are not well-known, but, assuming that they follow the trends of the disk stars in the Galaxy, these abundances are not constant with metallicity, which, if not taken properly into account, can produce an apparent variation of the relative abundances with metallicity (Proctor et al. 2004).

For all these reasons, in this work we do not attempt to derive relative abundances of the different elements. However, with the aim of exploring the behaviour of the different chemical species, we measure the metallicity using several indices that are especially sensitive to variations of different elements.

For the rest of the analysis, we make the assumption that the differences between the metallicities derived from various

[2] The so- called α-elements: O, Ne, Mg, Si, S, Ar, Ca, and Ti, are particles built up with α-particle nuclei.

index-index diagrams, combining Hβ with other metallicity indicators, are due to changes in the sensitivity of these indicators to variations of different chemical abundances.

3. The SSP-parameters σ relation

Figure 2 shows the ages and metallicities obtained in different index-index diagrams as a function of the velocity dispersion for both HDEGs (black symbols) and LDEGs (grey symbols). We have not plotted the dwarf galaxies of the sample, since it is not clear whether these galaxies are the faint extension of the giant ellipticals (see, for example, Gorgas et al. 1997; Pedraz et al. 2002; Graham & Guzmán 2003). Error-weighted linear fits to each subsample are also shown in the figure. These fits were derived by initially performing an unweighted ordinary least-squares regression of Y on X, and the coefficients from the first fit were then employed to derive (numerically, with a downhill method) the straight line data-fit with errors in both coordinates. Table 2 lists the slopes of the fits with their corresponding errors. The last two columns indicate the t-statistic obtained in the comparison of the slopes of HDEGs and LDEGs, and the probability that the slopes are different by chance. We analyse each panel separately:

- [M/H] (CN_2–Hβ) versus σ: while there is a correlation for the HDEGs between the metallicity and the velocity dispersion, this is not true for the LDEGs, which are compatible with a null relation. The most massive galaxies ($\sigma >$ 300 km s^{-1}), however, show the same behaviour in both environments, while for the rest of the galaxies, there exists a clear difference between the metallicity in the two galaxy subsamples.
- [M/H] (Fe4383–Hβ) versus σ: this panel shows a behaviour similar to the former one, that is, the correlation between the metallicity measured with Fe4383 and the velocity dispersion being stronger for HDEGs. For the LDEGs, however, the relation is almost flat and even slightly negative.
- [M/H] (Mgb-Hβ) versus σ: the relation between the metallicity measured with Mgb and the velocity dispersion is rather similar for both subsamples of galaxies. Furthermore, we did not find any significant difference between the zero point of both relations; both samples are compatible with the same metallicity (as measured with Mgb) σ relation.
- Age versus σ: in this panel, it can be seen that, while the relation is flat for the HDEGs, a correlation exists between the age and velocity dispersion for the LDEGs, in the sense that low velocity dispersion galaxies tend to be younger. This is in agreement with the suggestion by Trager et al. (2000b), who found differences in the (σ, t) plane between galaxies in the field and in the Fornax cluster. Interestingly, Jørgensen (1999) did not find any correlation between age and velocity dispersion in her study of a sample of galaxies in the Coma cluster, although she found a considerable dispersion in the ages of the galaxies. Caldwell et al. (2003) also found younger ages for lower σ galaxies in a sample of Virgo galaxies and galaxies in lower environments. Thomas et al. (2005) did not find a significant trend between the age and the velocity dispersion in either their sample of high- or low-density environment galaxies. However, they argued that the correlated errors of age and metallicity tend to dilute a correlation between age and the velocity dispersion and that their observational data are best reproduced by a relatively flat, but significant correlation.

  It is also clear from Fig. 2 that the age dispersion for less massive galaxies is higher than for the more massive ones, in agreement with other studies (e.g., Bender et al. 1993; Bressan et al. 1996; Worthey 1996; Mehlert et al. 1998; Vazdekis & Arimoto 1999; Jørgensen 1999; Smail et al. 2001; Caldwell et al. 2003).

As stated in Paper I, a decision was made to include the Virgo galaxies with the rest of the LDEGs to enlarge the number of galaxies in this group, as we did not find any difference between the stellar populations of those two sub-samples. In further support of this decision, we have plotted, in Fig. 3, the relation of the ages with the velocity dispersion for galaxies in the Coma cluster, Virgo clusters, and groups separately. As opposed to the behaviour of galaxies in the Fornax (Kuntschner 2000) and Coma clusters, those in the Virgo cluster show a greater spread in ages, the latter appearing to be correlated with their central velocity dispersion.

4. Simple stellar population or multiple bursts?

The new generation of stellar population models do not only predict individual features as a function of the age and metallicity, but synthesise full spectral energy distributions (SEDs) (Vazdekis 1999; Vazdekis et al. 2003; Bruzual & Charlot 2003; Le Borgne et al. 2004). This is possible thanks to the growing number of stellar libraries with a large number of stars (e.g., LeBorgne et al. 2003; Valdes et al. 2004; Sánchez-Blázquez et al. 2006b). To show the potential of these new models, in Fig. 4 we compare the spectral energy distribution of two galaxies, NGC 4467 and NGC 3605, with two synthetic spectra from V06 for a single population of age and metallicity, as indicated in the panels. Both observed and synthetic spectra were normalised to 5000 Å. As can be seen, the coincidence is very good. The shape of both spectra (observed and synthetic) are real, and their similarity gives support to the flux calibration of both the galaxies and the stellar spectra.

The age and metallicity values of the synthetic spectra that best reproduce the observed spectra were calculated by minimising the residual rms (obtained as the differences between the observed and the synthetic spectra in the region 3650−5150 Å). Internal reddening has not been taken into account in this analysis. The estimation of the synthetic spectra that best reproduce the observed is affected by the age-metallicity degeneracy. To show this, in Fig. 5, we have represented a grey-scale diagram with the rms of the residuals in the comparison of the synthetic spectra of different ages and metallicities with the spectrum of the galaxy NGC 4467. For this reason, we have computed the age and the metallicity by averaging the 9 best solutions weighted with the inverse of the residual variance of the comparison with the synthetic spectra. The last column of Table 5 shows the ages and metallicities obtained in this way for the sample of galaxies.

It has been seen in Sect. 3 that the LDEGs span a broad range in their apparent mean ages and that, in some cases, these ages are very low. Since the models assume a unique burst of star formation, these low values can indicate either that these galaxies are genuinely young, i.e., they formed all their stars recently, or that most of their stars were formed at early epochs, but that they have undergone later episodes of star formation involving a certain percentage of the total mass of the galaxy (see Trager et al. 2000b). In the latter case, the apparent mean age would depend on the relative light contributions of the different components to the considered spectral range. To distinguish between the two scenarios, we carried out a comparison of the observed galaxy spectra with the synthetic spectra extracted from the

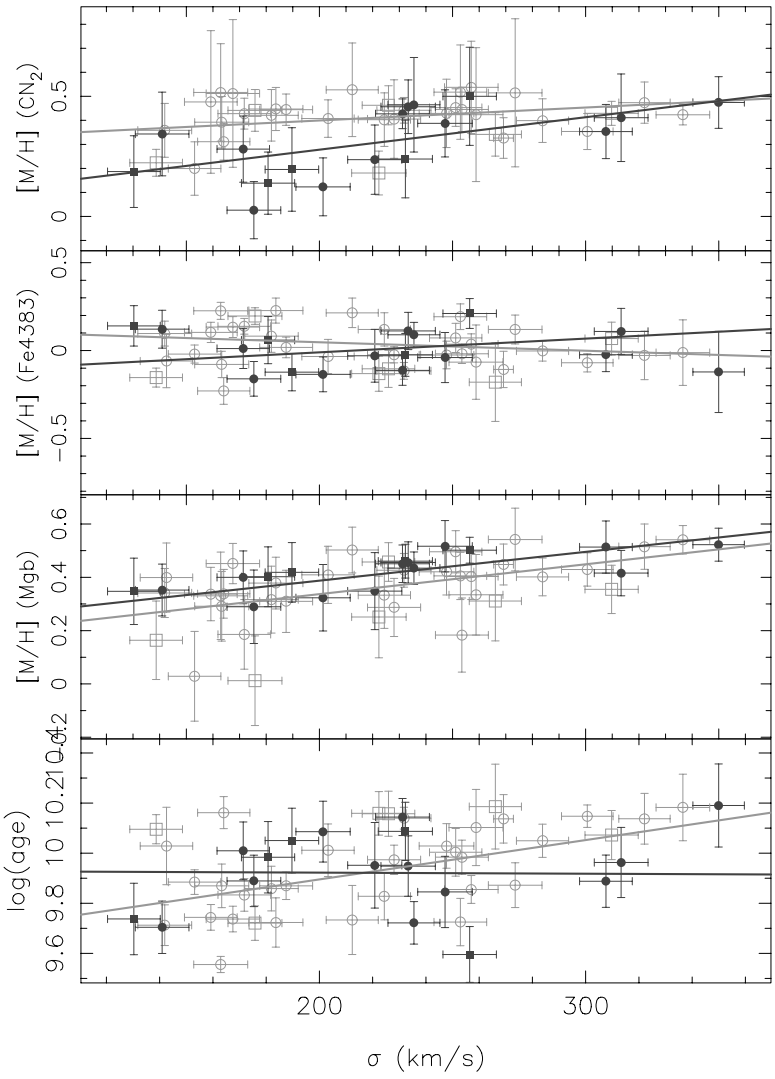

Fig. 2. Relations between metallicities, obtained with different indicators, and age against velocity dispersion for the sample of galaxies. Open symbols represent galaxies in low-density environments (LDEGs), while filled symbols indicate galaxies in high density environments (HDEGs). Squares correspond to S0 galaxies, while elliptical galaxies are represented with circles. Grey and black lines show the linear fit, weighting with the errors in both axes, to the LDEGs and HDEGs respectively.

Table 2. Slopes of the linear fits (b) and their errors (Δb) of the different parameters in Fig. 2 with the central velocity dispersion. The left side of the table shows the values for the LDEGs, while the right side of the table, the values for the HDEGs. The last two columns show the result of a t-test to verify if the slopes of both subsamples of galaxies are different. In particular, the last column shows the probability that the slopes of HDEGs and LDEGs are different by chance.

	LDEG		HDEG			
	b	Δb	b	Δb	t	α
[M/H] (CN_2)	0.00037	0.00034	0.00138	0.00065	1.37	9%
[M/H] (Fe4383)	−0.00050	0.00030	0.00085	0.00053	2.21	1%
[M/H] (Mgb)	0.00113	0.00031	0.00077	0.00042	0.69	24%
log (age)	0.00177	0.00033	0.00004	0.00064	2.41	1%

V06 models in two different wavelength ranges: 3650–4050 Å and 4750–5150 Å. The ages and metallicities were calculated combining the values of the 9 synthetic spectra that best reproduced the observed spectra in each wavelength interval, as explained above. Figures 6 and 7 show the age distributions obtained in both wavelength ranges for LDEG and HDEG, respectively. It is apparent from Fig. 6 that, for LDEGs, there is a significant difference between the ages obtained in the two different regions of the spectra. This is difficult to understand if all the stars were formed in a single burst, and it suggests that many LDEGs are composite systems consisting of an underlying old population plus, at least, a later star formation burst.

To study this in more detail, we have built different composite spectra in which we have added different components of metallicity [M/H] = +0.2 and ages ranging from 2.51 to 14.12 Gyr to an old population of 15.85 Gyr and metallicity [M/H] = −0.38 dex. The percentages of these two components were chosen to be 70 and 30% (model 1, solid line), 80 and 20% (model 2, dashed line), and 90 and 10% (model 3, dotted line) in mass, respectively. Figure 8 shows the relation between the derived ages in these two spectral ranges for different models and, over-plotted, the derived ages for the LDEGs (crosses). As can be seen, although is difficult to match the observed points with single scenarios, as the contribution in mass and the look-back time of the star formation event are highly degenerate, the combination of an old population and a burst of star formation would lead to similar trends in the derived ages as the observed for the LDEGs. We also note that, to reproduce the observed trends,

Table 3. Fraction of light contributed by a burst of star formation with a metallicity [M/H] = +0.2 and a strength of 20% in mass, in a galaxy with an age 15.85 Gyr and a metallicity [M/H] = −0.38 for different ages of the burst.

Age burst (Gyr)	fb (3650–4050 Å)	fb (4750–5150 Å)
1.00	0.956	0.932
1.12	0.944	0.917
1.26	0.932	0.904
1.41	0.920	0.896
1.58	0.900	0.879
1.78	0.852	0.817
2.00	0.811	0.766
2.24	0.766	0.712
2.51	0.712	0.685
2.82	0.653	0.634
3.16	0.596	0.588
3.55	0.544	0.547
3.98	0.482	0.493
4.47	0.430	0.449
5.01	0.398	0.409
5.62	0.343	0.362
6.31	0.284	0.307
7.08	0.246	0.268
7.98	0.193	0.217
8.91	0.161	0.188
10.00	0.135	0.162
11.22	0.110	0.140
12.59	0.084	0.109
14.12	0.070	0.093

the metallicity of the young component must be higher than the metallicity of the underlying old population, in agreement with the findings of other authors (e.g., Ferreras et al. 1999; Trager et al. 2000a; Thomas et al. 2005). We note here that the differences between the ages derived in the two spectral ranges do not follow a simple relation. The shape of this relation depends on the difference in the light contribution of the burst to the considered wavelength regions. Table 3 shows these fractions, as calculated in model 2. It can be noted that the contribution of the young population is higher in the red wavelength range than in the blue, when its age becomes older than 3.5 Gyr. This is due to the larger metallicity of the young component with respect to the subyacent population. In a model where both subyacent population and burst have the same metallicity, the contribution of the young component to the total light is always larger in the bluer wavelengths. Figure 9 shows the relation of the differences in the light fraction of the burst between the two considered spectral regions, and the age of the burst, also calculated for model 2. As can be seen, the differences are larger for older bursts (although the trend is not monotonic). That is why the differences between the ages calculated in two different spectral ranges increase with the age of the burst.

On the other hand, the distribution of ages for HDEGs (Fig. 7) shows no such clear dichotomy (see mean values in the insets). This is compatible with the idea that these galaxies constitute a more homogeneous (coeval) sample that have undergone their last episode of star formation at higher redshift. This interpretation is in agreement with our findings in Sánchez-Blázquez et al. (2003) and in Paper I.

5. The age-metallicity relation

Several authors have noted that when the age and metallicity obtained from an index-index diagram are plotted together, they

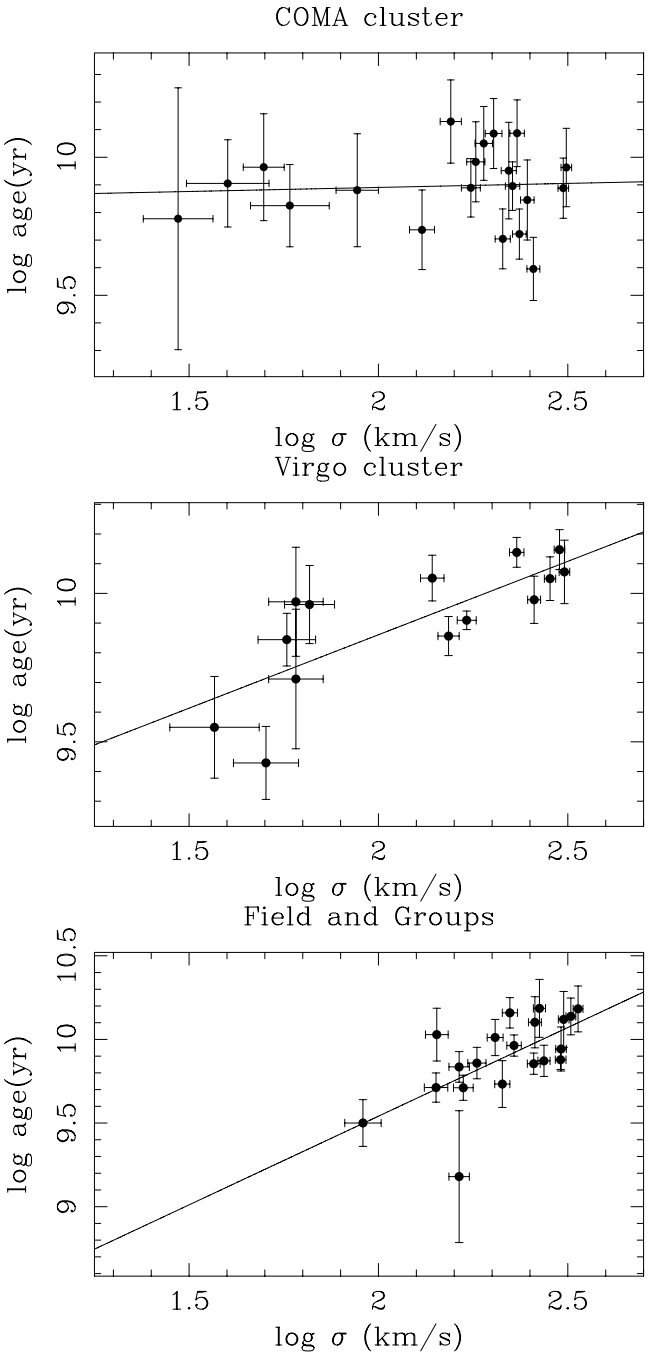

Fig. 3. Relation of the age with the velocity dispersion for galaxies in the Coma cluster, Virgo cluster, and galaxies in the field and poor groups.

show a correlation in the sense that younger galaxies seem to be also more metal rich (e.g., Trager et al. 1998; Jørgensen 1999; Ferreras et al. 1999; Trager et al. 2000b; Terlevich & Forbes 2002). This age-metallicity relation is difficult to explain under the hypothesis of passive evolution and high formation ages. However, this relation is expected if, during their evolution, galaxies have undergone several episodes of star formation, in which the new stars formed from pre-enriched gas by the previous generations of stars. Furthermore, the existence of an age-metallicity relation has implications in the interpretation of the scale-relations. The low dispersion in the Mg_2–σ or the color–magnitude relations and the existence of a fundamental plane have been common arguments in favour of the hypothesis that elliptical galaxies are old systems that formed all their

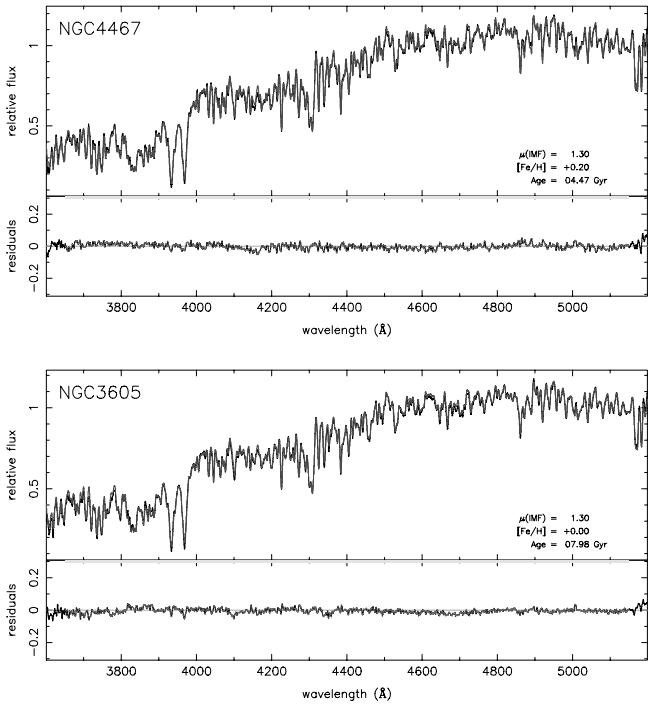

Fig. 4. Comparison of the observed spectra of the galaxies NGC 4467 and NGC 3605 (black line) and the synthetic spectra from V06 (grey line). The lower panels show the difference between both spectra. The parameters of the synthetic spectra are shown in the panel.

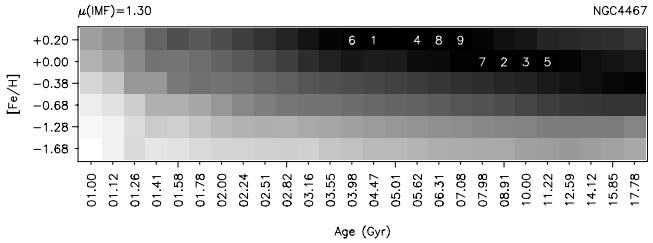

Fig. 5. Grey-scale diagram of the standard deviation in the residuals of the comparison of different synthetic spectra with the spectrum of NGC 4467. Darker squares represent lower residuals. The numbers indicate the combination of age and metallicity of the 9 best solutions, ordered from the lowest standard deviation (1) to the highest (9).

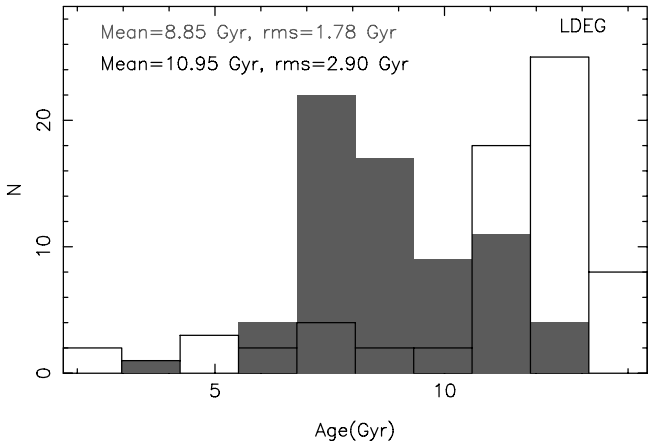

Fig. 6. Distribution of ages obtained comparing the synthetic spectra from V06 with the spectral energy distribution of LDEGs. The empty histogram shows the ages obtained with the comparison in the spectral range 4750–5150 Å, while the shaded histogram the ages obtained comparing the region from 3650–4050 Å.

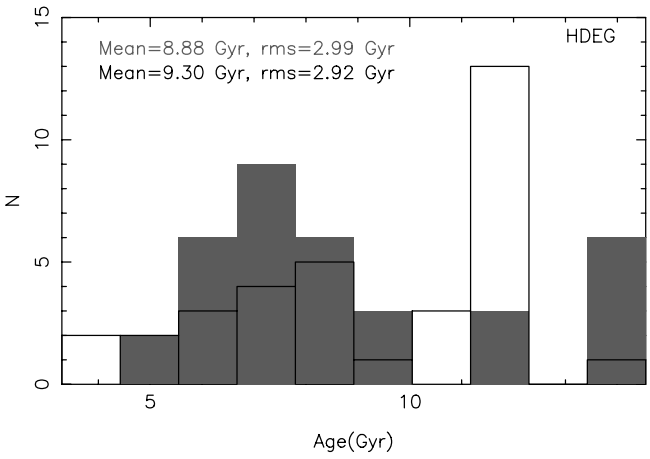

Fig. 7. Distribution of ages obtained by comparing the synthetic spectra from the models of V06 with the observed spectra for the sample of HDEGs. The empty histogram represents the ages obtained in the spectral range 4750–5150 Å while the shaded histogram shows the calculated ages in the spectral range 3650–4050 Å.

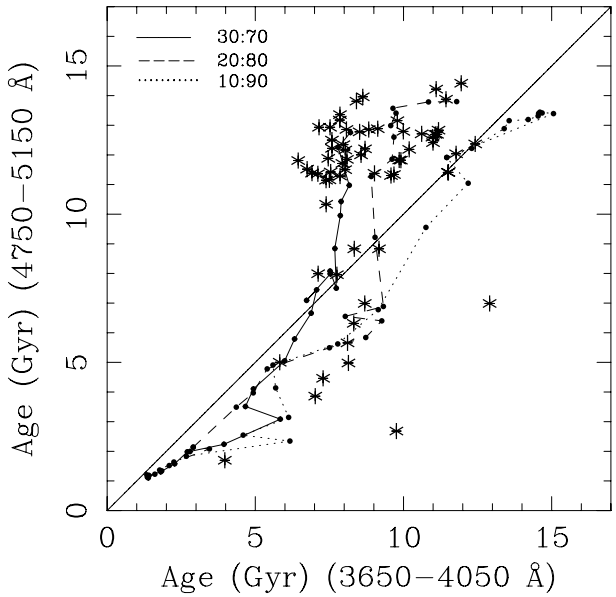

Fig. 8. Comparison of the ages derived in two different spectral ranges using the models of V06. The asterisks are the values calculated for the LDEG spectra, while the filled circles are the ages derived from the composite models in which two populations of different ages and metallicities are added (see text for details). The solid, dashed, and dotted lines connect the various two-component model combinations for the 30:70, 20:80, and 10:90 young:old population mass ratios, respectively. The age of the younger component increases from lower left to upper right of the diagram.

stars at high redshift and evolved passively since then (Bender et al. 1993; Bernardi et al. 1998). However, some authors, (e.g., Trager et al. 1998, 2000b; Ferreras et al. 1999; Jørgensen 1999) have studied the scale relationships showing that a possible age-metallicity degeneracy would constitute a conspiracy to preserve the low dispersion in those relationships even when a relatively large fraction of galaxies contain young stars.

Figure 10 shows this correlation for LDEGs when the age and metallicity are derived from a Fe4383–Hβ diagram. It is clear from this diagram that younger galaxies also appear to be more metal rich. However, when age and metallicity are

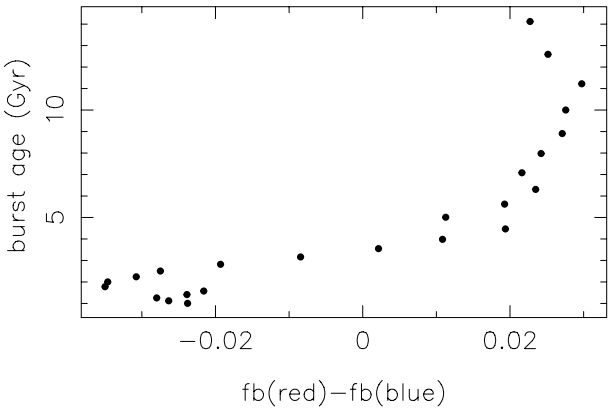

Fig. 9. Differences between the fraction of light contributed by a burst of star formation with metallicity $Z = +0.2$ in two different spectral ranges (4750−51500 Å) and (3650−4050 Å) when added to a population of age = 15.85 Gyr and metallicity $Z = -0.38$ for different ages of the burst.

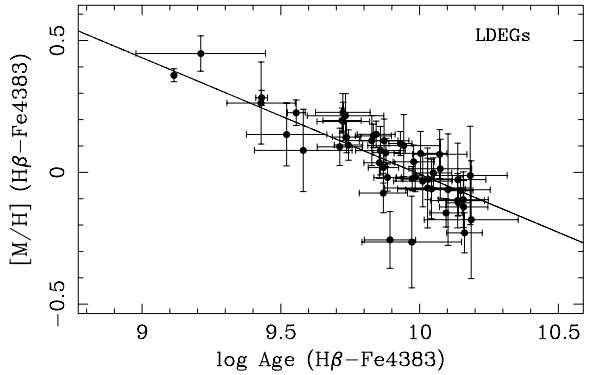

Fig. 10. Age-metallicity relation for LDEGs when the age and metallicity are derived from a Fe4383–Hβ diagram.

measured in a partially degenerated index-index diagram, the correlation of the errors in both parameters tends to create an artificial anti-correlation between them (Kuntschner et al. 2001), so it is difficult to disentangle whether the relation is real or an artifact due to the age-metallicity degeneracy. To check if the correlation of the errors could be the reason for the observed trend in our sample, we carried out a similar test to that performed by Kuntschner et al. (2001). We chose to model three different populations with the following characteristics:

(1) population with a single age of 8 Gyr and solar metallicity.
(2) population with a single age of 8 Gyr and metallicity ranging from [M/H] < 0.06 to [M/H] = 0.06.
(3) population with a range of ages between 5.6 and 10 Gyr, and solar metallicity.

We measured the Fe4383 and Hβ in these three populations and tried to reproduce the dispersion due to errors in this index-index diagram through Monte Carlo simulations. To do that, each point was perturbed with our typical observed error, following a Gaussian distribution. Figure 11 shows the index-index diagrams for 10 000 Monte Carlo realizations of the 3 populations (small dots). The model predictions from V06 are also plotted. The age and metallicities obtained by comparing the three different population with the models predictions are represented in the bottom panels of Fig. 11 (small dots). The grey circles represent the observed values in LDEGs.

We then performed a linear fit to quantify the slope of the relations in both the fake distributions and the galaxies. The errors in the slope were estimated using Monte Carlo simulations in which we generated N elements, (N being the number of points), where some data appear duplicated and others not. The final error was obtained as the standard deviation of the slopes in 1000 different simulations. The final results are shown in Table 4. We performed a t test to check whether the slopes of the simulations were compatible with the slope of the LDEGs data. A t value higher than 1.96 allows us to reject the hypothesis of equal slopes with a significance level lower than 0.05. As can be seen, the slopes defined by the populations 2 and 3 are not compatible with the slope of LDEGs. However, the slope obtained for the first distribution of constant age and metallicity is marginally compatible with the one obtained from the data (although the probability that the slopes are different is >95%). Nevertheless, none of the three models can reproduce the dispersion in age and metallicity observed in the sample of LDEGs. We then conclude that, although the correlation of the errors can explain the existence of an age-metallicity relation in a distribution of galaxies with constant age and metallicity, it cannot explain the observed dispersion in these parameters. If we try to reproduce the dispersion by simulating populations with a range in age or metallicity, the slope of the relation does not reproduce the slope obtained for the real galaxies. This indicates that part of the relation has to be real, and not only a consequence of the correlation of errors, although the actual value of the slope can be modified by this effect.

Another way to verify if the relation is an artifact of the error correlations is to represent the age versus the metallicity obtained in two completely independent index-index diagrams. Figure 12 shows the age-metallicity relation where the ages have been measured in a Hβ–Fe4531 diagram and the metallicities in a Hδ_F–Fe4383 diagram. A non-parametric Spearman rank-order correlation test gives a correlation coefficient of −0.47 corresponding to a significance level of 0.0002. Although the slope of the relation is flatter (-0.237 ± 0.076) than the one obtained by measuring the ages and metallicities in a Fe4383–Hβ diagram, there is still a significant correlation, which confirms that the age-metallicity relation is not entirely due to the correlation of the errors in both parameters.

The age-metallicity relation for HDEGs is plotted in Fig. 13 (see also Table 4). For comparison, we have also plotted the relation for the LDEGs (dashed line). As can be seen, the relation for HDEGs seems to be slightly flatter than for the LDEGs, although a t-test does not allow us to discard the possibility that they are equal within the errors. However, in Paper I we showed that to explain the relation of the indices with σ for the HDEGs, a variation of the age along the mass sequence was not necessary. Thus, if the age-metallicity relation is a consequence of recent star formation events (in which the younger stars have been formed from a more enriched gas), we would not expect to find this age-metallicity relation for the HDEGs. To verify whether the results obtained here are compatible with the relations of the indices with σ reported in Paper I, we carried out the following experiment:

– We calculated pairs of indices from the indices-σ relations obtained in Paper I at a variety of σ sampling from σ = 50 km s^{-1} to σ = 300 km s^{-1} in intervals of constant velocity dispersion. Then, we measured the age and metallicities of these fake distributions of indices. We did not try to reproduce the observed distribution, i.e., the number of points in each σ-bin, just the slope of the relation;

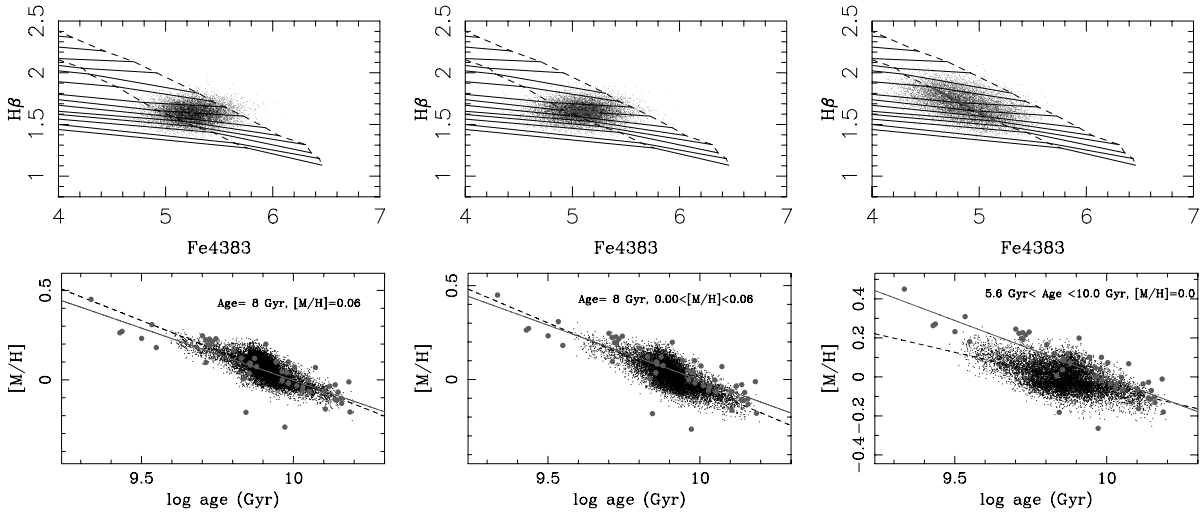

Fig. 11. *Top panels*: index-index diagrams for 3 different fake populations with the following characteristics: *from left to right*, (1) age 8 Gyr and solar metallicity [M/H] = 0; (2) age 8 Gyr and metallicity between 0.0 < [M/H] < 0.06; (3) age between 5.6 and 10 Gyr and solar metallicity [M/H] = 0. Small dots represent the results of the Monte Carlo simulations in which each point was perturbed following a Gaussian distribution with a standard deviation given by the typical error in Fe4383 and the Hβ indices in the sample of LDEGs. *Bottom panels*: age-metallicity relation for each of the 3 fake distributions plotted on the upper panels. Dashed lines show the linear fit to these distributions. Grey circles show the age and metallicity for LDEGs and the solid lines represent the linear fit to these data.

Table 4. Slopes of the age-metallicity relation calculated in the Fe4383–Hβ diagram for the three described distributions (see text), and for the LDEGs and HDEGs. The last two columns show the dispersion in age and metallicity for the different distributions and the subsamples of observed galaxies.

Distribution	Age (Gyr)	[M/H]	Slope	t	$\sigma_{\log(\mathrm{age})}$	$\sigma_{[\mathrm{M/H}]}$
1	8.00	0.06	-0.668 ± 0.005	2.00	0.084	0.073
2	8.00	0.00–0.06	-0.683 ± 0.005	2.37	0.084	0.076
3	5.62–10.00	0.00	-0.362 ± 0.004	5.41	0.113	0.069
LDEG			-0.516 ± 0.044		0.255	0.152
HDEG			-0.333 ± 0.152		0.181	0.153

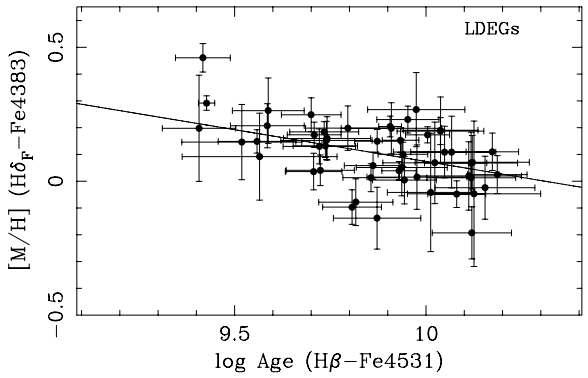

Fig. 12. Comparison of the ages and metallicities obtained from completely independent diagrams for the LDEGs. The line represents a least-square fit, minimizing the residuals in both directions, x and y.

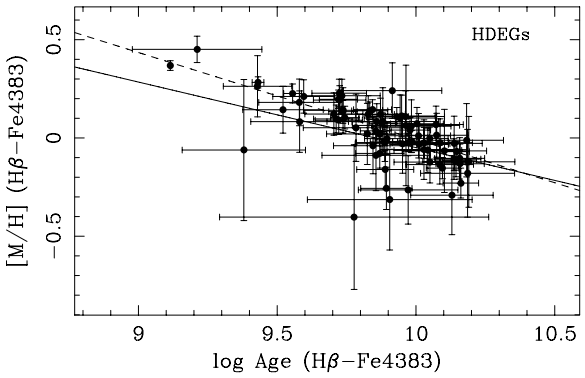

Fig. 13. Age-metallicity relation for HDEGs, where the age and the metallicity have been measured in a Fe4383–Hβ diagram. The solid line represents a least-square fit to the data minimising the residuals in both directions. The dashed line represents the best fit obtained for LDEGs.

– to measure the ages and metallicities of this mock sample, we use a Fe4383–Hβ diagram, obtaining the age-metallicity relation defined by the index-σ relations. The indices for each simulated point were then perturbed with the observational error adopting a Gaussian probability distribution, and an age-metallicity relation for the resultant distribution was also derived.

The age-metallicity relations obtained in this way are plotted in Fig. 14. We analyse the results obtained for LDEG and HDEG separately:

– LDEG: the age-metallicity relation obtained for the galaxies following the index-σ relation has an slope of $0.26 \times 10^{-5} \pm 10^{-5}$. This value is lower than the slope of the real data but the probability that it is significantly different than zero is higher than 99%. Interestingly, the slope obtained in this way is similar to the slope obtained with two independent

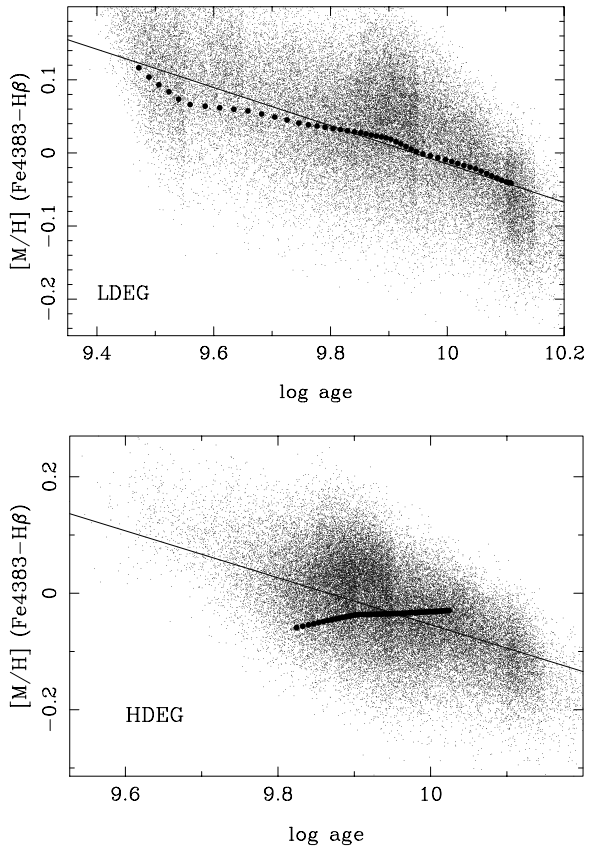

Fig. 14. Relation between the age and metallicity obtained for a mock distribution of points following the index-σ relations (filled circles) and for this sample, perturbed with the observational errors (small dots). See the text for details.

diagrams (-0.237 ± 0.076). We can consider this slope to be more representative of the real slope of the age-metallicity relation.

– HDEG: for this sample of galaxies, there is no age-metallicity relation for the points following the index-σ relations. However, when we add the errors, we obtain an artificial age-metallicity relation with a slope of $-0.403 \pm 6 \times 10^{-5}$, compatible, within the errors, with the slope obtained for the galaxies in this subsample.

Therefore, we conclude that a real relation between age and metallicity does exist (i.e., younger galaxies also tend to be more metal rich) for the LDEGs. On the other hand, HDEGs do not follow this relation, and the age-metallicity relation shown in Fig. 13 is probably a consequence of the correlation of the errors. In fact, when we measure the age and metallicity of the HDEGs in two independent diagrams (Fig. 15), we do not find any correlation between both parameters (the non-parametric Spearman rank order coefficient is 0.039 with a significance level of 0.422). The differences in the age-metallicity relation between LDEGs and HDEGs cannot be a consequence of differences in the luminosity ranges of the different samples because the luminosity coverage of the HDEGs is somewhat broader than that of LDEGs. A sample biased toward high-σ galaxies could also make the age-metallicity relation appear flatter, as there is some evidence that the age dispersion is higher in the range of low-σ galaxies (Poggianti et al. 2001b; Caldwell et al. 2003). The sample of HDEGs, however, is biased towards low-σ galaxies compared with the LDEGs (see Paper I).

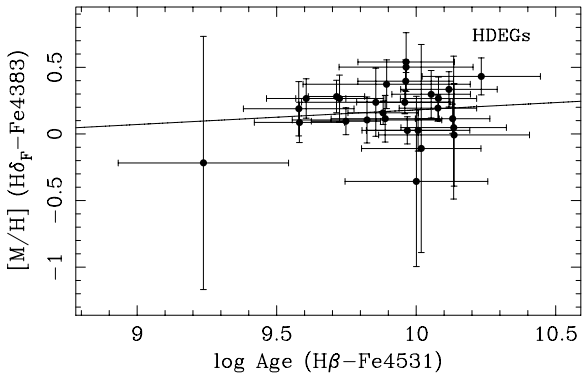

Fig. 15. Age metallicity relation for HDEGs where the age and the metallicity have been obtained from two independent diagrams. The line represent a least-square fit minimising the residuals in both directions, x and y.

6. Discussion

In this section, we will try to explain all the trends found in the previous sections with a common scenario. The results presented in this paper and in Paper I indicate that HDEGs constitute a more homogenous family than LDEGs; their stellar populations can be explained under the hypothesis of a single population, and they are, on average, older. In Fig. 2, it has been shown that this subsample of galaxies exhibits a relation between the metallicity and the velocity dispersion, no matter which indices are used to derive this parameter, but, on the contrary, there is no age variation with velocity dispersion. For LDEGs, however, the age dispersion is higher and their populations are best explained as a composition of different bursts of star formation.

The hierarchical clustering models of structure formation predict different star formation histories for galaxies situated in different environments (Baugh et al. 1996; Kauffmann & Charlot 1998; de Lucia et al. 2006). In these models, clusters of galaxies are formed from the highest peaks in the primordial density fluctuations. It is there where the merging of dark matter haloes, which contained the first galaxies, leads to galaxies dominated by a bulge at high redshifts ($z \geq 2$). The mergers of galaxies and the acquisition of cold gas cannot continue once the relative velocity dispersion between galaxies is higher than 500 km s^{-1}, which makes the occurrence of further star formation episodes in these galaxies more difficult. This truncated star formation history also explains the higher [Mg/Fe] found in HDEGs with respect to the values in younger looking LDEGs (Paper I).

On the other hand, the star formation in LDEGs has probably extended over a longer period of time, due to the occurrence of more star formation events or due to a longer single episode of star formation. This scenario was proposed to explain the differences between N, and maybe C, when comparing galaxies in different environments (Sánchez-Blázquez et al. 2003; Paper I).

We speculate that LDEGs and HDEGs could have initially presented similar relations between the metallicity and the velocity dispersion after their first massive star formation episode. However, if LDEGs have suffered subsequent episodes of star formation, the original correlation between metallicity and potential well (or mass) could have been erased, since other processes could have also played a role in defining the final metal content of the galaxies. The new stars, formed in the more recent events, would do it from a gas more enriched in the elements produced by low- and intermediate-mass stars, due to the higher active evolution timescale of these galaxies. If these star formation procesess have had a greater relative influence (a

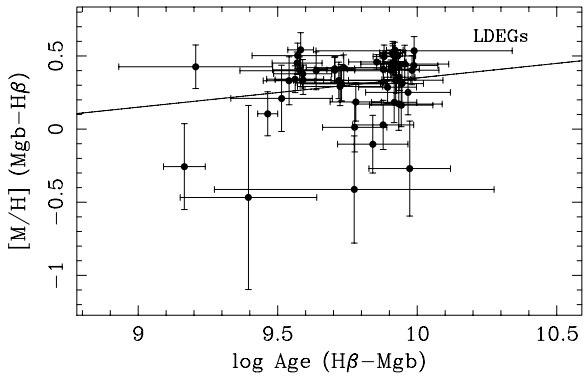

Fig. 16. Age-metallicity relation for the sample of low-density environment galaxies when these parameters are measured in a Mgb–Hβ diagram. The line indicate a least-square fit to the data, minimizing the residuals in both directions x and y.

larger ratio between the burst strength and the total galaxy mass) in less massive galaxies, as suggested by the age-σ relation, this would destroy the original relation between mass and metallicity (increasing Fe, C, and N in low velocity dispersion galaxies). Furthermore, this would result in a relation between age and metallicity (as inferred from Fe features) in LDEGs, but not in HDEGs, as it is found in this paper. Another posibility is that less massive galaxies have actually experienced a more extended star formation history than more massive galaxies (Chiosi & Carraro 2002). This latter possibility is favoured by some recent studies that found a depletion in the luminosity function of red galaxies towards the faint end (Smail et al. 2001; de Lucia et al. 2004).

Other authors have found differences between the mass-metallicity relation of galaxies in different environments. Trager et al. (2000b) found that there is a velocity dispersion-metallicity relation for old cluster galaxies, but no comparable relation exists for field ellipticals. This result is compatible with ours, with the difference that we still find a steep relation between the metallicity and the velocity dispersion for LDEGs when the metallicity is measured with Mgb. Actually, Trager et al. also found a relation between what they called the *enhanced* elements (including Mg) and velocity dispersion for all the galaxies in their sample.

If, as we have argued, the age-metallicity relation is a consequence of later episodes of star formation, and the relative enrichment has been more pronounced in the Fe-peak elements, we would expect differences in the age-metallicity relation when the metallicity is measured using an index with a different sensitivy to changes in Fe and Mg. Figure 16 shows the age-metallicity relation when these parameters are measured in a Mgb–Hβ diagram. The non-parametric rank order coefficient is 0.177, with a significance level of 0.10. Certainly, there is not a significant correlation between these two parameters when the Mgb index is used instead of Fe4383. We need to stress again that we are not calculating chemical abundances in this paper. The metallicity measured with Mgb does not correspond to the abundance of Mg, nor does the metallicity measured with Fe4383 correspond to a Fe abundance. We argue though, that the different behaviours of the metallicities calculated with different indices are the consequence of their different sensitivities to the variation of different chemical species. In this specific case, the flatter slope of the age-metallicity relation when a more (less) sensitive Mg (Fe) index is used is in agreement with our scenario.

Interestingly, the more massive galaxies in low density environments show a behaviour very similar to the massives galaxies of the Coma cluster. These very massive galaxies tend to have boxy isophotes, which can be explained by models of mergers without gas (Binney & Petrou 1985; Bender & Möllenhoff 1987; Nieto & Bender 1989; Nieto et al. 1991; Bender et al. 1992; Faber et al. 1997; Lauer et al. 2005), since a few percent of the mass in gas is sufficient to destroy boxy orbits and impart high global rotation (Barnes 1996; Barnes & Hernquist 1996). Furthermore, boxy galaxies tend to have flat inner profiles (Faber et al. 1997). N-body simulations of merging galaxies with central black holes (Ebisuzaki et al. 1991; Makino 1997; Quinlan & Hernquist 1997; Milosavljević & Merritt 2001) show that cores can indeed form in such merger remnants. Recently, Lauer et al. (2005) have found that power-law galaxies, on average, have steeper colour gradients than do core galaxies (although the difference is small). This result is compatible with the idea that power-law galaxies have formed in gas-rich mergers while core galaxies have formed from free-gas mergers, which would cause a dilution in the metallicity gradient. Actually, these mergers without gas have been observed in clusters at $z = 0.8$ (van Dokkum et al. 1999). The existence of these gas-free mergers indicates that the epoch of assembly does not necessarily coincide with the epoch of formation of the bulk of stars. This scenario could bring the hierarchical models of galaxy formation into agreement with the observed trends of age with mass for elliptical galaxies in LDEGs. These trends (low-σ galaxies appearing to be younger) are completely opposite to what is expected under these scenarios of galaxy formation, which predict that larger galaxies assemble at later times than small ones (Kauffman et al. 1993). However, these predictions are made under the assumption that all the gas cooled off and formed stars when the haloes were assembled. However, other processes, such as supernova feedback, may play a role in regulating the rate at which stars form in these systems (e.g., Kawata & Gibson 2003). Several mechanisms have been proposed to explain the appearance that low-mass galaxies have suffered a more extended star formation history. Kawata (2001) suggests that UV background radiation is a possible candidate because it suppresses cooling and star formation more strongly in lower mass systems (Efstathiou 1992), and is expected to extend the duration of star formation. Chiosi & Carraro (2002) have recently built N-body-tree-SPH simulations incorporating cooling, star formation, energy feedback, and chemical evolution. These authors find that the star formation history is governed by the initial density and total mass of the galaxy, and that the interplay of the above processes results in a more extended star formation history in low-mass galaxies. Until we understand the role of these mechanisms completely, we will not be able to rule out different processes of galaxy formation.

7. Conclusions

We have studied the stellar population properties of the centres of 98 early-type galaxies spanning a large range in velocity dispersion. Using the new stellar population synthesis models of V06, which include a new and improved stellar library (MILES), we have derived ages and metallicities for this sample of galaxies. Due to the difficulties in deriving chemical abundances with the available tools, we have studied the behaviours of the different chemical elements in a very qualitative way, measuring the metallicity with different indices especially sensitive to different chemical species. From this analysis, we conclude:

– The sample of LDEGs spans a wide range in SSP-equivalent ages and metallicities. This confirms previous results

obtained by other authors (e.g., González 1993; Trager et al. 1998; Trager et al. 2000b). This age spread is not meant to imply that galaxies formed all their stars at different epochs. In fact, we have shown that galaxies in low density environments are best explained as a composition of populations in which a low percentage of young stars is added to an old population, in agreement with the conclusions of Trager et al. (2000b).

- For the subsample of LDEGs, there is a relation between the age and the velocity dispersion in the sense that less massive galaxies tend to be younger. This "down-sizing effect" suggests either that the episodes of star formation have had a larger relative influence on the low mass galaxies, or that the last star formation activity occurs on average at lower redshifts for progressively fainter galaxies. This relation is also present for galaxies in the Virgo cluster, but it is not present in the subsample of galaxies in the Coma cluster.
- Comparing the ages obtained in different regions of the spectra, we have shown that galaxies in low-density environments are best described by a composition of populations in which a small percentage of young stars are added to an old population. On the other hand, the population of the HDEGs can be described with a single burst, which does not necessarily indicate that these galaxies formed all their stars in a single burst, but may indicate that the last episode of star formation finished at an earlier time than in LDEGs.
- The sample of LDEGs shows a relation between the age and the metallicity implying that younger galaxies are also more metal rich. This relation is true even when the age and metallicity are measured in completely independent index-index diagrams, indicating that it is not a consequence of a correlation of the errors in both parameters. However, the actual relation can be flatter than the relation derived from a partially degenerate index-index diagram. We have shown that this relation is only evident when some indicators are used to measure the metallicity. In particular, we do not find a relation when the metallicity is measured in a Mgb–Hβ diagram. If the age-metallicity relation is a consequence of the occurrence of late star formation in these galaxies, this would imply that the relative enrichment in Mg in the last generations of stars is much less important with respect to the Fe. The sample of HDEGs, however, do not show this relation between the age and the metallicity, which is in agreement with the general picture exposed in this work (and in Paper I), in which HDEGs have had a truncated star formation history compared to their counterparts in low-density environments.
- A mass-metallicity relation for HDEGs exists, in the sense that more massive galaxies also tend to be more metal rich. This is independent of the indicator used to measure the metallicity, although the absolute value of the slope is somewhat smaller if Fe4383 is used instead of Mgb or CN_2. However, in the case of the LDEGs, the mass-metallicity relation is only apparent when the metallicity is measured with Mgb. When the metallicity is measured with Fe4383 or CN_2, younger galaxies tend to lie at higher metallicities for a given σ. This can indicate that the mass-metallicity relation is a consequence of processes that occurred when the bulk of the stars were formed. In LDEGs, later star formation events raise the metallicity in low-mass systems, flattening this relation. As the relative enrichment in these events is more pronounced in the elements produced by low-mass stars, the flattening in the relation, when the metallicity is measured with indices sensitives to these elements, is also more evident.

Our results show that differences exist in the stellar populations of galaxies inhabitating different environments. HDEGs represent a more homogenous sample of galaxies than LDEGs; their stellar populations can be explained assuming a single burst and their mean ages are slightly higher. On the other hand, LDEGs show more variety in their stellar populations. They span a large range of ages and their spectral features are better explained, assuming that they have suffered multiple bursts of star formation.

It is worth recalling that the results discussed in Papers I and II of this series refer only to the central regions of the galaxies. If significant radial age and metallicity gradients are present within the galaxies, these results cannot be considered representative of the whole star formation history. That is, to constrain the star formation history of early-type galaxies, we cannot ignore the behaviour of the SSP-parameters along the radii. This analysis is beyond the scope of the present paper, but will be the subject of the third paper of the series.

Acknowledgements. We are very grateful to the referee, Jim Rose, for his very constructive report and many useful suggestions. We are also grateful to Javier Cenarro, Brad Gibson, Reynier Peletier, Daisuke Kawata, and Alexandre Vazdekis for many fruitful discussions. The Calar Alto Observatory is operated jointly by the Max-Planck Insitute für Astronomie, Heidelberg, and the Spanish Instituto de Astrofísica de Andalucía (CSIC). This work was supported by the Spanish research project AYA 2003-01840 and by the Australian Research Council. We are grateful to the CAT for generous allocation of telescope time.

References

Baugh, C. M., Cole, S., & Frenk, C. S. 1996, MNRAS, 283, 1361
Bender, R., & Möllenhoff, C. 1987, A&A, 177, 71
Bender, R., Burstein, D., & Faber, S. M. 1992, ApJ, 399, 462
Bender, R., Burstein, D., & Faber, S. M. 1993, ApJ, 411, 153
Bernardi, M., Renzini, A., da Costa, L. N., et al. 1998, ApJ, 508, L143
Bressan, A., Chiosi, C., & Tantalo, R. 1996, A&A, 311, 425
Binney, J., & Petrou, M. 1985, MNRAS, 214, 449
Bruzual, G., & Charlot, S. 2003, MNRAS, 344, 1000
Buzzoni, A. 1995, ApJS, 98, 69
Caldwell, N. 1983, ApJ, 268, 90
Caldwell, N., Rose, J. A., & Concannon, K. D. 2003, AJ, 125, 2891
Cardiel, N., Gorgas, J., Sánchez-Blázquez, P., et al. 2003, A&A, 409, 511
Chiosi, C., & Carraro, G. 2002, MNRAS, 335, 335
Cole, S., Aragón-Salamanca, A., Frenk, C. S., Navarro, J. F., & Zepf, S. E. 1994, MNRAS, 271, 781
Côté, P., West, M. J., & Marzke, R. O. 2002, ApJ, 567, 853
De Lucia, G., Poggianti, B. M., Aragón-Salamanca, et al. 2004, ApJ, 610, L77
De Lucia, G., Springel, V., White, S. D. M., Croton, D., & Kauffmann, G. 2006, MNRAS, 366, 499
Dressler, A., Oemler, A. Jr, Couch, W. J., Smail, I., et al. 1997, ApJ, 490, 577
Ebisuzaki, T., Makino, J., & Okumura, S. K. 1991, Nature, 354, 212
Efstathiou, G. 1992, MNRAS, 256, P43
Faber, S. M., Tremaine, S., Ajhar, et al. 1997, AJ, 114, 1771
Faber, S. M., Trager, S. C., González, J. J., & Worthey, G. 1999, A&AS, 267, 273
Ferreras, I., Charlot, S., & Silk, J. 1999, ApJ, 521, 81
Fisher, D., Franx, M., & Illingworth, G. 1995, ApJ, 448, 119
González, J. J. 1993, Ph.D. Thesis, University of California
Gorgas, J., Pedraz, S., Guzmán, R., Cardiel, N., & González, J. J. 1997, ApJ, 481, L19
Graham, A. W., & Guzmán, R. 2003, AJ, 125, 2936
Gregg, M. D. 1989, ApJ, 337, 45
Jones, L., Smail, I., & Couch, W. J. 2000, ApJ, 528, 118
Jørgensen, I. 1997, MNRAS, 288, 161
Jørgensen, I. 1999, MNRAS, 306, 607
Kauffmann, G. 1996, MNRAS, 281, 487
Kauffmann, G., & White, S. D. M. 1993, MNRAS, 261, 921
Kauffmann, G., & Charlot, S. 1998, MNRAS, 294, 705
Kauffman, G., White, S. D. M., & Guiderdoni, B. 1993, MNRAS, 264, 201
Kawata, D. 2001, ApJ, 558, 598
Kawata, D., & Gibson, B. K. 2003, MNRAS, 340, 908
Kuntschner, H. 2000, MNRAS, 315, 184
Kuntschner, H., & Davies, R. L. 1998, MNRAS, 295, L29
Kuntschner, H., Lucey, J. R., Smith, R. J., Hudson, M. J., & Davies, R. L. 2001, MNRAS, 323, 615

Kuntschner, H., Smith, R. J., Colless, M., et al. 2002, MNRAS, 337, 172
Kyplin, A., Hoffman, Y., Kravtsov, A. V., & Gottlöber, S. 2003, ApJ, 596, 19
Lauer, T. R., Faber, S. M., Gebhardt, K., et al. 2005, AJ, 129, 2138
Le Borgne, J.-F., Bruzual, G., Pelló, et al. 2003, A&A, 402, 433
Le Borgne, D., Rocca-Volmerange, B., Prugniel, P., Lanǫn, A., Fioc, M., & Soubiran, C. 2004, A&A, 425, 881
Makino, J. 1997, ApJ, 478, 58
Mehlert, D., Bender, R., Saglia, R. P., & Wegner, G. 1998, in Untangling Coma Berenices: A New Vision of an Old Cluster, ed. A. Mazure, F. Casoli, F. Durret, & D. Gerbal (Word Scientific Publishing Co. Pte. Ltd.), 107
Mehlert, D., Thomas, D., Saglia, R. P., Bender, R., & Wegner, G. 2003, A&A, 407, 423
Milosavljević, M., & Merritt, D. 2001, ApJ, 563, 34
Moore, B., Ghigna, S., Governato, F., et al. 1999, ApJ, 524, L19
Nieto, J.-L., & Bender, R. 1989, A&A, 215, 266
Nieto, J.-L., Bender, R., & Surma, P. 1991, A&A, 244, L37
O'Connell, R. W. 1976, ApJ, 206, 370
Pedraz, S., Gorgas, J., Cardiel, N., Sánchez-Blázquez, P., & Guzmán, R. 2002, MNRAS, 332, L59
Peletier, R. F., Ph.D. Thesis, University of Groningen
Poggianti, B. M., Bridges, T. J., Mobasher, B., et al. 2001a, ApJ, 562, 689
Poggianti, B. M., Bridges, T. J., Carter, D., et al. 2001b, ApJ, 563, 118
Proctor, R. N., Forbes, D. A., Hau, G. K. T., et al. 2004, MNRAS, 349, 1381
Quinlan, G. D., & Hernquist, L. 1997, New Astron., 2, 533
Salaris, M., & Weiss, A. 1998, A&A, 335, 943
Salaris, M., Chieffi, A., & Straniero, O. 1993, ApJ, 414, 580
Salasnich, B., Girardi, L., Weiss, A., & Chiosi, C. 2000, A&A, 361, 1023
Sánchez-Blázquez, P. 2004, Ph.D. Thesis, Universidad Complutense de Madrid
Sánchez-Blázquez, P., Gorgas, J., Cardiel, N., Cenarro, A. J., & González, J. J. 2003, ApJ, 590, L91
Sánchez-Blázquez, P., Gorgas, J., Cardiel, N., & González, J. J. 2006a, A&A, 457, 787 (Paper I)
Sánchez-Blázquez, P., Peletier, R. F., Jiménez, J., et al. 2006b, MNRAS [arXiv:astro-ph/0607009]
Smail, I., Kuntschner, H., Kodama, T., et al. 2001, MNRAS, 323, 839
Steinmetz, M., & Navarro, J. 2002, New Astron., 7, 155
Somerville, R. S., & Primack, J. R. 1999, MNRAS, 310, 1087
Tantalo, R., Chiosi, C., & Bressan, A. 1998, A&A, 333, 419
Terlevich, A. I., & Forbes, D. A. 2002, MNRAS, 330, 547
Thomas, D., & Maraston, C. 2003, A&A, 401, 429
Thomas, D., Maraston, C., & Bender, R. 2003, MNRAS, 343, 279
Thomas, D., Maraston, C., & Korn, A. 2004, MNRAS, 351, L19
Thomas, D., Maraston, C., Bender, R., & Mendes de Oliveira, C. 2005, ApJ, 623, 673
Trager, S. C., Ph.D. Thesis, University of California
Trager, S. C., Worthey, G., Faber, S. M., Burstein, D., & González, J. J. 1998, ApJS, 116, 1
Trager, S. C., Faber, S. M., Worthey, G., & González, J. J. 2000a, AJ, 119, 1645
Trager, S. C., Faber, S. M., Worthey, G., & González, J. J. 2000b, AJ, 120, 165
Trager, S. C., Faber, S. M., & Dressler, A. 2001, in Astrophysical Ages and Times Scales, ed. T. von Hippel, C. Simpson, & N. Manset, ASP. Conf. Ser., 245, 429
Tripicco, M., & Bell, R. A. 1995, AJ, 110, 3035
Valdes, F., Gupta, R., Rose, J. A., Singh, H. P., & Bell, D. J. 2004, ApJS, 152, 251
van Dokkum, P. G., Franx, M., Fabricant, D., Kelson, D. D., & Illingworth, G. D. 1999, ApJ, 520, L95
Vazdekis, A. 1999, ApJ, 513, 224
Vazdekis, A., & Arimoto, N. 1999, ApJ, 525, 144
Vazdekis, A., Kuntschner, H., Davies, R. L., Arimoto, N., Nakamura, O., & Peletier, R. F. 2001, ApJ, 551, L127
Vazdekis, A., Cenarro, A. J., Gorgas, J., Cardiel, N., & Peletier, R. F. 2003, MNRAS, 340, 1317
Worthey, G. 1994, ApJS, 95, 107
Worthey, G. 1996, in New light on galaxy evolution, ed. R. Bender, & R. L. Davies, Kluwer Academic Publishers, IAU Symp., 171, 71
Worthey, G. 1998, PASP, 110, 888
Worthey, G., & Ottaviani, D. L. 1997, ApJS, 111, 377
Ziegler, B. L., Bower, R. G., Smail, I., Davies, R. L., & Lee, D. 2001, MNRAS, 325, 1571

Online Material

Table 5. Central ages and metallicities obtained in different index-index diagrams. The associated errors are indicated under the measurements. See Sect. 2 for more details.

Galaxy	log (age)	[M/H]	log (age)	[M/H]	log (age)	[M/H]	log (age)	[M/H]	log (age)	[M/H]
	[MgbFe]–Hβ		Fe4383–Hβ		Mgb–Hβ		CN_2–Hβ		(spectral synthesis)	
NGC 221	9.455	0.164	9.431	0.283	9.464	0.105	9.443	0.223	9.698	−0.003
	0.029	0.087	0.021	0.028	0.036	0.150	0.263	0.202	0.066	0.053
NGC 315	9.913	0.517			9.913	0.517	9.931	0.411	10.066	0.079
	0.028	0.053			0.028	0.053	0.032	0.036	0.039	0.031
NGC 507	9.996	0.196	10.186	−0.180	9.945	0.311	9.938	0.342	10.078	0.093
	0.091	0.129	0.169	0.223	0.077	0.150	0.105	0.091	0.038	0.032
NGC 584	9.748	0.213	9.828	0.120	9.719	0.333	9.704	0.403	9.790	0.125
	0.110	0.085	0.094	0.095	0.162	0.125	0.161	0.111	0.046	0.031
NGC 636	9.768	0.207	9.859	0.082	9.727	0.316	9.703	0.421	9.701	0.110
	0.104	0.082	0.089	0.092	0.162	0.126	0.160	0.107	0.042	0.032
NGC 821	9.714	0.299	9.733	0.215	9.571	0.502	9.568	0.527	10.063	0.113
	0.180	0.183	0.138	0.084	0.163	0.086	0.159	0.195	0.044	0.032
NGC 1600	9.935	0.300	10.075	0.014			9.807	0.442	10.094	0.120
	0.052	0.060	0.113	0.112			0.120	0.042	0.035	0.032
NGC 1700	9.706	0.283	9.725	0.193	9.579	0.405	9.561	0.517	9.833	0.131
	0.076	0.071	0.095	0.073	0.097	0.089	0.031	0.196	0.046	0.030
NGC 2300	9.905	0.289	9.943	0.101			9.869	0.438	9.927	0.136
	0.100	0.083	0.129	0.118			0.062	0.148	0.046	0.030
NGC 2329	10.153	0.127			9.955	0.445	10.122	0.168	9.923	0.060
	0.155	0.197			0.158	0.129	0.128	0.134	0.061	0.053
NGC 2693	10.173	0.197			9.988	0.435	10.027	0.357	9.988	0.131
	0.114	0.084			0.086	0.094	0.064	0.060	0.044	0.030
NGC 2694	9.931	0.162	10.029	−0.059	9.638	0.399	9.920	0.212	9.726	0.165
	0.195	0.158	0.155	0.152	0.273	0.130	0.155	0.161	0.040	0.024
NGC 2778	9.704	0.288	9.737	0.134	9.569	0.452	9.561	0.512	10.016	0.100
	0.071	0.061	0.051	0.060	0.089	0.076	0.029	0.307	0.039	0.032
NGC 2832	9.949	0.334	10.138	−0.027	9.913	0.515	9.764	0.474	9.988	0.131
	0.075	0.098	0.101	0.138	0.035	0.085	0.229	0.086	0.045	0.031
NGC 3115	9.923	0.297	10.050	−0.002	9.906	0.402	9.752	0.399	9.931	0.133
	0.025	0.056	0.066	0.057	0.029	0.071	0.135	0.091	0.046	0.031
NGC 3377	9.715	0.084	9.712	0.097	9.562	0.341	9.560	0.359	9.950	−0.010
	0.089	0.097	0.081	0.071	0.102	0.092	0.102	0.112	0.071	0.068
NGC 3379	9.914	0.172	9.974	−0.024	9.894	0.287	9.865	0.405	9.935	0.129
	0.033	0.059	0.059	0.046	0.104	0.109	0.119	0.163	0.046	0.031

Table 5. continued.

Galaxy	log (age)	[M/H]	log (age)	[M/H]	log (age)	[M/H]	log (age)	[M/H]	log (age)	[M/H]
	[MgbFe]–Hβ		Fe4383–Hβ		Mgb–Hβ		CN_2–Hβ		(spectral synthesis)	
NGC 3605	9.512	0.227	9.521	0.144	9.514	0.210			9.925	0.012
	0.142	0.187	0.145	0.119	0.182	0.227			0.071	0.064
NGC 3608	9.926	0.176	10.011	−0.033	9.878	0.409	9.829	0.407	9.921	0.122
	0.078	0.085	0.105	0.097	0.129	0.107	0.125	0.078	0.040	0.031
NGC 3641	9.742	0.216	9.870	−0.079	9.723	0.292	9.702	0.392	10.105	0.107
	0.099	0.083	0.087	0.075	0.153	0.131	0.150	0.107	0.034	0.032
NGC 3665	10.105	0.014	10.159	−0.131	9.967	0.251	10.003	0.181	9.910	0.045
	0.132	0.188	0.087	0.100	0.152	0.153	0.108	0.091	0.065	0.052
NGC 3818	9.761	0.218	9.870	0.018	9.729	0.310	9.597	0.444	10.077	0.099
	0.090	0.071	0.055	0.059	0.147	0.117	0.083	0.065	0.039	0.033
NGC 4261	9.709	0.423	9.879	0.075			9.582	0.544	10.095	0.118
	0.141	0.069	0.047	0.053			0.140	0.316	0.034	0.032
NGC 4278	10.095	0.152			9.931	0.500	9.968	0.372	10.066	0.079
	0.080	0.072			0.063	0.042	0.038	0.050	0.039	0.031
NGC 4365	9.900	0.344	9.978	0.040			9.881	0.414	10.100	0.139
	0.084	0.065	0.074	0.064			0.065	0.139	0.035	0.030
NGC 4374	10.054	0.118	10.148	−0.069	9.925	0.429	9.941	0.354	10.017	0.099
	0.103	0.105	0.045	0.052	0.029	0.062	0.083	0.075	0.039	0.032
NGC 4415	9.855	–0.146	9.893	−0.256	9.841	−0.103			9.751	−0.424
	0.104	0.118	0.092	0.108	0.126	0.197			0.062	0.079
NGC 4431	10.001	–0.408	9.972	−0.264	9.973	−0.270			9.955	−0.483
	0.125	0.243	0.179	0.174	0.146	0.325			0.067	0.069
NGC 4464	10.057	–0.060	10.096	−0.154	9.943	0.164	9.929	0.223	9.846	0.115
	0.085	0.100	0.058	0.054	0.113	0.147	0.038	0.056	0.046	0.032
NGC 4467	9.993	0.027	10.043	−0.063	9.934	0.171	9.917	0.254	9.851	0.116
	0.130	0.135	0.122	0.113	0.156	0.180	0.119	0.134	0.046	0.031
NGC 4472	9.984	0.220	10.072	0.068	9.935	0.355	9.921	0.429	10.098	0.139
	0.084	0.078	0.098	0.094	0.056	0.090	0.077	0.050	0.035	0.030
NGC 4478	9.874	0.055	9.885	−0.020	9.878	0.029	9.851	0.199	9.699	0.093
	0.067	0.088	0.049	0.051	0.109	0.168	0.081	0.111	0.044	0.034
NGC 3379	9.914	0.172	9.974	−0.024	9.894	0.287	9.865	0.405	9.935	0.129
	0.033	0.059	0.059	0.046	0.104	0.109	0.119	0.163	0.046	0.031
NGC 3605	9.512	0.227	9.521	0.144	9.514	0.210			9.925	0.012
	0.142	0.187	0.145	0.119	0.182	0.227			0.071	0.064
NGC 3608	9.926	0.176	10.011	−0.033	9.878	0.409	9.829	0.407	9.921	0.122
	0.078	0.085	0.105	0.097	0.129	0.107	0.125	0.078	0.040	0.031
NGC 3641	9.742	0.216	9.870	−0.079	9.723	0.292	9.702	0.392	10.105	0.107
	0.099	0.083	0.087	0.075	0.153	0.131	0.150	0.107	0.034	0.032

Table 5. continued.

Galaxy	log (age)	[M/H]	log (age)	[M/H]	log (age)	[M/H]	log (age)	[M/H]	log (age)	[M/H]
	[MgbFe]–Hβ		Fe4383–Hβ		Mgb–Hβ		CN_2–Hβ		(spectral synthesis)	
NGC 3665	10.105	0.014	10.159	−0.131	9.967	0.251	10.003	0.181	9.910	0.045
	0.132	0.188	0.087	0.100	0.152	0.153	0.108	0.091	0.065	0.052
NGC 3818	9.761	0.218	9.870	0.018	9.729	0.310	9.597	0.444	10.077	0.099
	0.090	0.071	0.055	0.059	0.147	0.117	0.083	0.065	0.039	0.033
NGC 4261	9.709	0.423	9.879	0.075			9.582	0.544	10.095	0.118
	0.141	0.069	0.047	0.053			0.140	0.316	0.034	0.032
NGC 4278	10.095	0.152			9.931	0.500	9.968	0.372	10.066	0.079
	0.080	0.072			0.063	0.042	0.038	0.050	0.039	0.031
NGC 4365	9.900	0.344	9.978	0.040			9.881	0.414	10.100	0.139
	0.084	0.065	0.074	0.064			0.065	0.139	0.035	0.030
NGC 4374	10.054	0.118	10.148	−0.069	9.925	0.429	9.941	0.354	10.017	0.099
	0.103	0.105	0.045	0.052	0.029	0.062	0.083	0.075	0.039	0.032
NGC 4415	9.855	–0.146	9.893	−0.256	9.841	−0.103			9.751	−0.424
	0.104	0.118	0.092	0.108	0.126	0.197			0.062	0.079
NGC 4431	10.001	–0.408	9.972	−0.264	9.973	−0.270			9.955	−0.483
	0.125	0.243	0.179	0.174	0.146	0.325			0.067	0.069
NGC 4464	10.057	–0.060	10.096	−0.154	9.943	0.164	9.929	0.223	9.846	0.115
	0.085	0.100	0.058	0.054	0.113	0.147	0.038	0.056	0.046	0.032
NGC 4467	9.993	0.027	10.043	−0.063	9.934	0.171	9.917	0.254	9.851	0.116
	0.130	0.135	0.122	0.113	0.156	0.180	0.119	0.134	0.046	0.031
NGC 4472	9.984	0.220	10.072	0.068	9.935	0.355	9.921	0.429	10.098	0.139
	0.084	0.078	0.098	0.094	0.056	0.090	0.077	0.050	0.035	0.030
NGC 4478	9.874	0.055	9.885	−0.020	9.878	0.029	9.851	0.199	9.699	0.093
	0.067	0.088	0.049	0.051	0.109	0.168	0.081	0.111	0.044	0.034
NGC 4486b					9.981	0.403	9.993	0.380	9.989	0.130
					0.096	0.099	0.069	0.064	0.044	0.031
NGC 4489	9.437	0.223	9.429	0.263	9.206	0.426	9.429	0.265	9.787	0.149
	0.126	0.179	0.123	0.156	0.276	0.149	0.270	0.230	0.045	0.028
NGC 4552	10.094	0.100			9.933	0.431	9.752	0.488	9.949	0.121
	0.091	0.115			0.034	0.064	0.258	0.097	0.045	0.031
NGC 4564	9.904	0.256	9.931	0.109	9.854	0.459			10.025	0.117
	0.031	0.055	0.042	0.046	0.100	0.049			0.046	0.032
NGC 4594			10.102	−0.066	9.923	0.334	9.805	0.424	10.101	0.118
			0.152	0.212	0.169	0.151	0.203	0.279	0.033	0.031
NGC 4621	9.942	0.299	10.140	−0.115	9.917	0.426	9.772	0.442	10.057	0.115
	0.038	0.050	0.044	0.048	0.027	0.063	0.137	0.053	0.044	0.032
NGC 4636	10.011	0.181	10.158	−0.104	9.918	0.458	9.770	0.463	9.894	0.122
	0.121	0.104	0.090	0.105	0.042	0.073	0.220	0.081	0.047	0.031

Table 5. continued.

Galaxy	log (age)	[M/H]	log (age)	[M/H]	log (age)	[M/H]	log (age)	[M/H]	log (age)	[M/H]
	[MgbFe]–Hβ		Fe4383–Hβ		Mgb–Hβ		CN_2–Hβ		(spectral synthesis)	
NGC 4673	9.577	0.297	9.722	0.090	9.556	0.434	9.552	0.465	9.891	0.059
	0.207	0.164	0.085	0.071	0.027	0.061	0.034	0.197	0.066	0.051
NGC 4692	9.908	0.305	9.948	0.112	9.872	0.456	9.726	0.457	9.984	0.131
	0.127	0.083	0.121	0.106	0.052	0.077	0.196	0.111	0.045	0.031
NGC 4697	9.770	0.197	9.833	0.138	9.780	0.186	9.599	0.428	10.042	0.108
	0.082	0.072	0.065	0.045	0.092	0.131	0.082	0.064	0.044	0.033
NGC 4742	9.018	0.489	9.115	0.368					9.509	−0.007
	0.109	0.093	0.003	0.024					0.064	0.075
NGC 4839	9.732	0.423	9.915	0.241			9.732	0.425	9.911	0.126
	0.205	0.097	0.178	0.141			0.235	0.132	0.041	0.031
NGC 4842A	9.925	0.327	10.087	−0.024	9.904	0.460	9.945	0.239	9.953	0.120
	0.107	0.079	0.116	0.122	0.033	0.063	0.154	0.162	0.045	0.031
NGC 4842B	9.934	0.189	9.984	0.060	9.659	0.402	9.947	0.139	9.783	0.113
	0.140	0.121	0.143	0.134	0.251	0.112	0.145	0.129	0.046	0.032
NGC 4875	9.922	0.182	10.050	−0.123	9.732	0.419	9.920	0.196	9.973	0.122
	0.103	0.101	0.129	0.106	0.191	0.112	0.150	0.174	0.051	0.031
NGC 4864	9.885	0.272	9.952	−0.029	9.867	0.348	9.892	0.236	9.852	0.077
	0.117	0.101	0.171	0.150	0.151	0.144	0.156	0.144	0.072	0.052
NGC 4865	9.726	0.340	9.888	−0.023	9.586	0.513	9.723	0.353	9.830	0.128
	0.159	0.077	0.104	0.096	0.375	0.098	0.172	0.113	0.047	0.031
NGC 4867	9.720	0.294	9.845	−0.039	9.572	0.517	9.700	0.387	9.805	0.012
	0.256	0.216	0.142	0.143	0.178	0.096	0.177	0.140	0.075	0.064
NGC 4874	9.923	0.253	9.963	0.109	9.893	0.416	9.818	0.411	9.883	0.133
	0.088	0.091	0.140	0.131	0.053	0.085	0.148	0.182	0.045	0.030
NGC 4889	9.963	0.302	10.190	−0.121	9.912	0.523	9.752	0.474	9.988	0.131
	0.187	0.114	0.166	0.231	0.047	0.062	0.297	0.108	0.044	0.031
NGC 4908	9.977	0.077	10.086	−0.135	9.910	0.323	9.954	0.123	9.923	0.091
	0.127	0.123	0.121	0.099	0.119	0.125	0.064	0.120	0.041	0.032
NGC 5638	9.715	0.232	9.744	0.104	9.591	0.337	9.565	0.477	9.843	0.147
	0.073	0.069	0.051	0.058	0.100	0.100	0.030	0.297	0.045	0.029
NGC 5796	9.852	0.235	9.872	0.120	9.582	0.542	9.588	0.515	9.942	0.145
	0.103	0.150	0.089	0.082	0.046	0.118	0.148	0.308	0.045	0.029
NGC 5812	9.728	0.310	9.843	0.144	9.705	0.413			10.037	0.128
	0.089	0.057	0.068	0.050	0.071	0.084			0.045	0.032
NGC 5813	9.741	0.242	9.855	0.036	9.704	0.403	9.575	0.537	10.084	0.110
	0.087	0.064	0.056	0.059	0.072	0.086	0.026	0.192	0.039	0.032
NGC 5831	9.543	0.316	9.556	0.226	9.541	0.331	9.511	0.516	9.937	0.127
	0.130	0.160	0.032	0.048	0.093	0.164	0.041	0.203	0.046	0.031

Table 5. continued.

Galaxy	log (age)	[M/H]	log (age)	[M/H]	log (age)	[M/H]	log (age)	[M/H]	log (age)	[M/H]
	[MgbFe]–Hβ		Fe4383–Hβ		Mgb–Hβ		CN_2–Hβ		(spectral synthesis)	
NGC 5845	9.919	0.172	9.984	−0.018	9.917	0.183	9.723	0.445	10.065	0.112
	0.064	0.108	0.068	0.056	0.081	0.139	0.131	0.092	0.044	0.033
NGC 5846	9.926	0.219	10.029	−0.025	9.737	0.421	9.884	0.429	10.049	0.103
	0.048	0.061	0.089	0.079	0.134	0.087	0.070	0.142	0.044	0.032
NGC 5846A	10.029	0.077	10.162	−0.230	9.925	0.338	9.931	0.311	9.893	0.122
	0.103	0.111	0.064	0.076	0.052	0.092	0.074	0.076	0.047	0.031
NGC 6127	9.927	0.273	10.004	0.072	9.881	0.496	9.734	0.453	9.925	0.136
	0.042	0.061	0.095	0.083	0.039	0.079	0.190	0.078	0.047	0.030
NGC 6166					9.989	0.536	10.197	0.310	10.099	0.001
					0.352	0.097	0.197	0.166	0.038	0.047
NGC 6411	9.718	0.252	9.723	0.228	9.589	0.378	9.576	0.447	10.104	0.107
	0.093	0.078	0.098	0.071	0.104	0.097	0.094	0.090	0.035	0.033
NGC 6482					10.040	0.445	10.162	0.364	10.058	0.116
					0.130	0.025	0.076	0.023	0.044	0.032
NGC 6577	9.947	0.279	10.137	−0.107	9.913	0.448	9.936	0.326	9.953	0.116
	0.073	0.071	0.097	0.103	0.045	0.077	0.089	0.085	0.045	0.031
NGC 6702			9.211	0.451			9.314	0.538	9.996	0.119
			0.233	0.067			0.130	0.094	0.046	0.031
NGC 6703	9.745	0.092	9.721	0.197	9.776	0.012	9.570	0.442	9.945	0.125
	0.097	0.092	0.069	0.047	0.115	0.168	0.027	0.087	0.045	0.031
NGC 7052									10.073	0.096
									0.038	0.032
IC 767	9.397	–0.478	9.344	−0.107	9.395	−0.468			9.279	−0.240
	0.173	0.296	0.131	0.308	0.245	0.630			0.045	0.102
IC 794	9.731	–0.184	9.581	0.083	9.774	−0.413	9.807	0.442	9.788	−0.072
	0.175	0.188	0.176	0.156	0.501	0.366	0.120	0.042	0.069	0.059
IC 832	9.797	0.091	9.889	−0.161	9.720	0.290	9.827	0.026	9.756	−0.066
	0.097	0.109	0.103	0.099	0.158	0.138	0.266	0.119	0.068	0.065
IC 3957	9.957	0.108	10.009	0.011	9.743	0.400	9.915	0.280	10.150	0.162
	0.126	0.116	0.115	0.113	0.147	0.099	0.111	0.138	0.029	0.026
IC 3959	9.733	0.324	9.895	−0.003			9.703	0.455	10.083	0.112
	0.111	0.063	0.081	0.081			0.168	0.114	0.039	0.032
IC 3963	9.721	0.211	9.737	0.141	9.591	0.347	9.727	0.187	9.837	0.021
	0.144	0.106	0.143	0.115	0.152	0.124	0.150	0.149	0.077	0.062
IC 3973	9.569	0.342	9.595	0.211	9.546	0.502	9.547	0.500	9.834	0.133
	0.103	0.061	0.111	0.085	0.033	0.048	0.041	0.204	0.046	0.030

Table 5. continued.

Galaxy	log (age)	[M/H]	log (age)	[M/H]	log (age)	[M/H]	log (age)	[M/H]	log (age)	[M/H]
	[MgbFe]–Hβ		Fe4383–Hβ		Mgb–Hβ		CN_2–Hβ		(spectral synthesis)	
IC 4026	9.723	0.270	9.825	0.021	9.707	0.347	9.773	0.128	10.149	0.149
	0.259	0.223	0.147	0.156	0.181	0.140	0.158	0.206	0.029	0.028
IC 4042					10.216	0.188			10.151	0.152
					0.149	0.141			0.029	0.028
IC 4051	9.965	0.315			9.912	0.540	9.921	0.489	9.911	0.130
	0.152	0.099			0.034	0.056	0.038	0.043	0.041	0.030
CGCG 159-41	10.112	0.089			9.936	0.435	9.970	0.327	9.890	0.127
	0.113	0.141			0.047	0.073	0.130	0.115	0.047	0.031
CGCG 159-43	9.994	0.188	10.144	−0.112	9.915	0.451	9.919	0.427	10.148	0.155
	0.106	0.095	0.074	0.085	0.037	0.071	0.086	0.062	0.028	0.027
CGCG 159-83									9.993	−0.172
									0.067	0.068
CGCG 159-89	9.573	0.258	9.704	0.122	9.558	0.352	9.559	0.343	10.101	0.114
	0.218	0.189	0.105	0.108	0.116	0.097	0.215	0.174	0.034	0.032
DRCG 27-032	10.187	−0.137			10.177	−0.119			10.014	−0.143
	0.219	0.415			0.226	0.650			0.061	0.067
DRCG 27-127	9.703	0.323	9.784	0.052	9.572	0.471	9.762	0.097	10.106	0.108
	0.172	0.104	0.190	0.171	0.219	0.096	0.160	0.169	0.034	0.032
DRCG 27-128	9.585	0.157	9.580	0.181	9.556	0.320			9.960	0.092
	0.154	0.121	0.146	0.119	0.159	0.155			0.045	0.032
GMP 3121	10.104	−0.247	9.964	0.064	10.115	−0.291			9.610	−0.050
	0.222	0.381	0.193	0.307	0.248	0.695			0.071	0.082
GMP 3196	9.936	−0.339	9.856	−0.088	9.874	−0.138			9.655	−0.325
	0.284	0.229	0.195	0.180	0.229	0.286			0.072	0.094
MCG+05-31-63	10.053	−0.061	10.130	−0.291	9.933	0.196			9.920	−0.107
	0.142	0.214	0.149	0.201	0.229	0.208			0.073	0.071
PGC 126756	9.957	−0.507	9.905	−0.314	9.969	−0.552			9.656	−0.329
	0.176	0.363	0.297	0.256	0.190	0.652			0.072	0.093
PGC 126775	9.411	−0.275	9.380	−0.061	9.396	−0.163	9.307	0.311	9.559	−0.369
	0.249	0.387	0.222	0.359	0.359	0.802	0.281	0.174	0.059	0.099
RB 91	9.873	0.127	9.880	0.084	9.726	0.353	9.880	0.086	10.151	0.152
	0.190	0.154	0.201	0.172	0.212	0.152	0.145	0.254	0.029	0.028
RB 113									10.153	0.156
									0.029	0.027